Published in final edited form as:

Nature. 2009 March 12; 458(7235): 201–205. doi:10.1038/nature07843.

Distinct sensory representations of wind and near-field sound in the *Drosophila* brain

Suzuko Yorozu[1,3], **Allan Wong**[1,3], **Brian J. Fischer**[1], **Heiko Dankert**[1,2], **Maurice J. Kernan**[4], **Azusa Kamikouchi**[5,6], **Kei Ito**[5], and **David J. Anderson**[1,3,7]

[1] Division of Biology 216-76, California Institute of Technology, Pasadena, CA 91125

[2] Division of Engineering and Applied Sciences 136-93, California Institute of Technology, Pasadena, CA 91125

[3] Howard Hughes Medical Institute, California Institute of Technology, Pasadena, CA 91125

[4] Department of Neurobiology and Behavior, SUNY Stony Brook, Stony Brook, NY 11794-5239

[5] Institute of Molecular and Cellular Biosciences, University of Tokyo, Yayoi, Bunkyo-ku, Tokyo 113-0032 Japan

[6] Sensory System Lab, Institute of Zoology, University of Cologne, 50923 Cologne, Germany

Abstract

Behavioral responses to wind are thought to play a critical role in controlling the dispersal and population genetics of wild *Drosophila* species1,2, as well as their navigation in flight3, but their underlying neurobiological basis is unknown. We show that *Drosophila melanogaster*, like wild-caught *Drosophila* strains4, exhibits robust wind-induced suppression of locomotion (WISL), in response to air currents delivered at speeds normally encountered in nature1,2. Here we identify wind-sensitive neurons in Johnston's Organ (JO), an antennal mechanosensory structure previously implicated in near-field sound detection (reviewed in5,6). Using Gal4 lines targeted to different subsets of JO neurons7, and a genetically encoded calcium indicator8, we show that wind and near-field sound (courtship song) activate distinct populations of JO neurons, which project to different regions of the antennal and mechanosensory motor center (AMMC) in the central brain. Selective genetic ablation of wind-sensitive JO neurons in the antenna abolishes WISL behavior, without impairing hearing. Different neuronal subsets within the wind-sensitive population, moreover, respond to different directions of arista deflection caused by airflow and project to different regions of the AMMC, providing a rudimentary map of wind-direction in the brain. Importantly, sound- and wind-sensitive JO neurons exhibit different intrinsic response properties: the former are phasically activated by small, bi-directional, displacements of the aristae, while the

[7]Author for correspondence: Tel: (626) 395-6821, Fax: (626) 564-8243, e-mail: wuwei@caltech.edu.

AUTHOR CONTRIBUTIONS

S.Y. and D.J.A. designed experiments, S.Y. carried out all experiments reported in this paper and D.J.A. and S.Y. wrote the manuscript. A.W. wrote Matlab programs for DF/F measurements and mechanical probe actuation, B.J.F. assisted with computational filtering of song stimuli, H.D. assisted with computational and statistical analysis of data, M.J.K. provided facilities and support for electrophysiological experiments, and A.K. and K.I. provided Gal4 lines.

latter are tonically activated by unidirectional, static deflections of larger magnitude. These different intrinsic properties are well suited to the detection of oscillatory pulses of near-field sound and laminar airflow, respectively. These data identify wind-sensitive neurons in JO, a structure that has been primarily associated with hearing, and reveal how the brain can distinguish different types of air particle movements, using a common sensory organ.

We observed that *Drosophila* exhibit a rapid and reversible arrest of walking activity under gentle air currents (0.7–1.6 m/s) (Fig. 1a, b; Supplemental Movie 1). This behavior is also exhibited by wild-caught *Drosophila* species, at wind speeds (1.7 m/s – 2.8 m/s) within the range measured in their natural habitats1,2,4 (J.S. Johnston, personal communication; Supplementary Footnote S1). This behavior, called wind-induced suppression of locomotion (WISL), could be observed whether or not locomotor activity was enhanced by mechanical startle prior to the introduction of airflow (Fig. 1b, 3d). Importantly, WISL was not observed in response to near-field sound stimuli such as courtship song (280 Hz pulse song – 75–100 dB9) (Supplemental Fig. S1a).

Recent antennal-gluing experiments have implicated the antenna, and by extension JO, in wind-sensation in *Drosophila*3,10. Surgical removal of the third antennal segment (a3), or gluing of a3 to the second antennal segment (a2), both of which cause a functional impairment of JO11, eliminated WISL (Fig. 1c, d). Genetic ablation of mechanosensory chordotonal neurons using nanchung-Gal412 and *UAS-hid*, a *Drosophila* cell death gene13, also eliminated WISL (Supplemental Figure S1b–d). Taken together, these results support the idea that JO is required for WISL, a conclusion confirmed by genetic ablation of specific JO subpopulations (see Fig. 3, below).

To investigate how wind and sound are discriminated by the brain, we first performed extracellular recordings from the antennal nerve14. In some electrode placements, spike trains were evoked by both wind (0.3–0.9m/s) and courtship song (pulse-song) (Fig. 1e–h). The short duration of the wind-evoked action potentials (<1 msec) is consistent with neuronal, rather than muscle, action potentials15. In other cases, responses were evoked by sound but not wind (Fig. 1i, j; a few spikes were detected at the onset and offset of the wind stimulus), or by wind but not sound (Fig. 1k, l). These results suggested that different axons within the antennal nerve might respond differentially to wind vs. sound.

To determine whether distinct subsets of JO neurons are activated by wind vs. near-field sound, we performed functional imaging experiments, using a genetically encoded calcium sensor (GCaMP-1.38), controlled by different Gal4 enhancer trap lines expressed in JO7. These lines identify 5 major groups of JO axonal projections in the AMMC, called zones A, B, C, D, and E (Fig. 2a, inset). Each Gal4 driver labels a subset of zones, but mosaic analysis has revealed that individual JO neurons innervate only one zone 7. Since it is difficult to distinguish the cell bodies of these 5 groups of neurons in JO itself, we imaged activity in JO axon terminals in the AMMC, where the 5 zones are easily discriminated. To do this, we mounted live *Drosophila* in an inverted orientation under a 2-photon microscope, while airflow and/or near-field sound were delivered from tubing and a speaker, respectively (Fig. 2b).

Using an enhancer trap line (JO-AB) that selectively labels neurons in zones A and B7 we observed strong GCaMP activation by courtship song (pulse song; 400 Hz, 90 dB SPL16), but not by wind (0.9 m/s) (Supplemental Fig. S2a–e). Conversely, using a different line (JO-CE) that selectively labels zones C and E7 we observed responses to airflow, but not to courtship song (Supplemental Fig. S2f–j). To directly compare responses to wind and sound in the same preparation, we employed a third line, which labels neurons in zones A, C and E7 (Fig. 2c). These experiments confirmed that zone A was activated by sound but not by airflow, while zone E was activated by airflow but not by sound (Fig. 2d–i, and Supplemental Movie 2a, b). The same selective responses were observed when the two stimuli were presented sequentially or simultaneously (Fig. 2j–o, and Supplemental Movie 2c, d). Together, these data indicated that JO contains distinct populations of sound- and wind-responsive neurons that project to different regions of the AMMC7 (Supplementary Footnote S2).

To determine whether the wind-sensitive JO neurons are also required for WISL behavior, we genetically ablated these neurons using a toxin, Ricin A chain17. Because the JO-CE Gal4 driver is expressed not only in JO neurons but also in the central brain (Fig. 3a), we employed an intersectional strategy to restrict ablation to the antenna using *eyeless-FLP* recombinase. The specificity of this manipulation was confirmed using a FLP-dependent mCD8GFP reporter18 (Fig. 3b).

Following ablation of JO-C and -E neurons, WISL behavior was eliminated (Fig. 3g), while basal locomotor activity (prior to wind exposure) and phototaxis behavior were unaffected (Fig. 3g, 3i, Supplemental Fig. S3a). Importantly, female flies lacking JO-CE neurons had normal hearing, as evidenced by their unperturbed receptivity to courtship by wild-type males, a behavior that depends on the females' ability to hear male courtship song. In contrast, females lacking *nanchung*, a gene required for hearing12, or whose aristae were glued to their head11, exhibited a greatly increased latency to copulation (Fig. 3h, Nan/Nan; Bi-Gl). These data indicate that JO-CE neurons are necessary for WISL behavior, but dispensable for a hearing-dependent behavior.

We next investigated the functional significance of the two wind-sensitive JO subpopulations (C and E). Axons innervating zones C and E terminate in lateral vs. medial domains of the AMMC, respectively (Fig. 4a, b, c). When airflow was applied to the front of the head (0°), or at 45°, there was strong activation in zone E, and little activation in zone C. Conversely, airflow applied from the rear (180°) activated zone C, and slightly inhibited zone E (Fig. 4d–f, and Supplemental movie 3a–c). Airflow applied to the side of the head (90°) activated zone C ipsilaterally, and zone E contralaterally (Fig. 4d–f, 90°; Supplemental movie 3d). Thus zone C and E neurons are differentially sensitive to airflow directionality.

High magnification video analysis (Supplemental movie 4a–c) suggested a simple hypothesis to account for these observations: airflow from different directions moves the aristae either anteriorly or posteriorly (Fig. 4g), and the direction of arista deflection determines whether zone C or E neurons are activated (Fig. 4j). Arista ablation experiments indicated that the activation of wind-sensitive JO neurons, like that of sound-sensitive JO neurons11,19, is dependent upon this structure (Supplemental Figure S4). To test the

hypothesis directly, we moved the aristae in different directions using a probe controlled by a DC motor (Fig. 4h). Displacing the arista posteriorly with a probe activated the E zone almost as strongly as wind delivered from the front, and weakly inhibited the C zone (Fig. 4i, “Push back”), while displacing it anteriorly activated the C zone and inhibited the E zone (Fig. 4i, “Push forward”). These data demonstrate that zones C and E are sensitive to different directions of arista deflection. This model can explain the asymmetric activation of zones C and E in ipsi- and contral-lateral hemi-brains during wind stimulation from 90° (Fig. 4f–g, 90°), because this stimulus produces opposite deflection of the aristae on the ipsi- and contra-lateral sides of the head (Fig. 4g, 90°, Supplemental movie 4d). An internal comparison of activity between zones C and E, both within and between each hemi-brain, could provide a basis for computing wind direction3.

What stimulus features are responsible for the selective activation of sound vs. wind-sensitive neurons in JO? We first asked whether these two classes of mechanoreceptors are sensitive to different stimulus amplitudes, i.e., air particle velocities (v_{air}). A pressure gradient microphone positioned at the antenna9 yielded a v_{air} = 0.011 m/s for the 400 Hz sound stimulus played at 90dB, which maximally activated JO-AB neurons (Fig. 5a). Yet this sound stimulus did not activate zone E neurons (Supplementary Figure S2g), even though these neurons are activated by airflow at a v_{air} as low as 0.005 m/s (Fig. 5b). Thus, the selectivity of JO-CE and -AB neurons for wind vs. sound is not simply due to differences in stimulus magnitude.

We next asked whether JO-AB and -CE neurons might have different intrinsic sensitivities to different types of arista movements, by moving the aristae in steps of different magnitudes and patterns using a probe controlled by a DC motor (Fig. 5c–d). Sound-sensitive neurons in zone A (Fig. 5f, red traces), were activated by displacements as small as 0.01 mm (Fig. 5e, red hatched bars), while wind-sensitive neurons in zone E (Fig. 5g, green traces) were only weakly activated at displacements below 0.04 mm (Fig. 5e, green bars). Thus, zone A neurons have a lower displacement threshold than zone E neurons (see also Fig. 5i, l).

Strikingly, we observed that zone E neurons remained active for as long as the aristae were displaced, while zone A neurons were only transiently activated at the onset and offset of probe displacement (Fig. 5j, m). This suggested that zone E neurons might adapt slowly, and therefore respond tonically, while zone A neurons might adapt rapidly, and therefore respond phasically. To confirm this, we moved the aristae in three successive steps of 0.033 mm each (total displacement of 0.099 mm; Fig. 5k). Zone A neurons exhibited transient (phasic) responses after each displacement (Fig. 5n, red traces), while zone E neurons were tonically activated for the duration of each displacement, and were maximally activated after the second step (Fig. 5n, green traces). These data indicate that JO-AB and JO-CE neurons respond phasically and tonically to arista displacement, with low vs. high activation thresholds, respectively (see Supplementary Footnote S3). Furthermore, zone A neurons were activated by bidirectional movements, while zone E neurons were activated only unidirectionally (Fig. 5j, m). These different intrinsic response properties are well matched to the oscillatory arista movements caused by pulses of near-field sound vs. uni-directional arista deflections caused by wind. The fly’s ability to discriminate wind vs. sound using a

common sensory organ is thus explained by different population of JO neurons with different intrinsic response properties, which project to distinct area of the AMMC.

The identification of different subpopulations of JO neurons with tonic vs. phasic response properties illustrates a general and conserved feature of mechanosensation. In mammalian skin, slowly adapting, tonically activated Merkel cells20, and rapidly adapting, phasically activated Meissner's corpuscles21 are used for different types of light touch sensation. In *Drosophila*, these two properties have been adapted to detect different types of bulk air particle movements by different subsets of JO neurons. In the accompanying paper, Kamikouchi et al.22 demonstrate, using complementary imaging methods, that zone AB neurons are activated by sound and required for hearing. They also show that zone CE neurons are required for the behavioral response to gravity (negative gravitaxis), a force that could also produce static deflections of the arista, albeit of a smaller magnitude than those produced by wind (Supplemental Footnote S4).

The data presented here indicate that JO is not simply a hearing organ6, but also mediates wind detection, in a direction sensitive manner. Wind-activated neurons in JO are, moreover, required for an innate behavioral response to wind. The function of WISL in nature is not clear. Field studies have suggested that wind is a major environmental factor affecting the dispersal of wild *Drosophila* populations1,2,4. WISL may have evolved to control population dispersal, and thereby maintain genetic homogeneity1,2. Alternatively, WISL may represent a defense mechanism that serves to protect individual flies from injury, or to prevent dispersal from food resources. Identification of the sensory neurons that mediate WISL opens the way to a systematic analysis of the genes and neural circuitry that underlie this robust, innate behavioral response to wind.

METHODS SUMMARY

Behavioral assay

20 flies were used for each WISL trial. A standard WISL trial lasts for 270 seconds. During the first 55 seconds, the flies' baseline locomotor activity was recorded. Where indicated, at t=55 seconds, a brief mechanical stimulus was applied to transiently increase the flies' locomotor activity. Airflow exposure was then initiated, at t=80 seconds, and terminated at t=200 seconds.

Electrophysiology

Sample preparation and electrophysiological recordings from Johnston's organ axons were performed as described14.

Calcium response imaging

Flies were anesthetized in a plastic vial on ice for 15–20 seconds, and then gently inserted into a hole of a thin plastic rectangular plate. After stabilizing the fly with a small drop of wax (55°C), the proboscis and the area surrounding the proboscis were surgically removed, in a saline bath, to expose the ventral side of the brain. The preparation was then mounted on a microscope in an inverted orientation for calcium response imaging. The antennae were

kept intact and dry throughout the exposure to different stimuli (sound, wind and mechanical probe displacement).

Detailed descriptions of fly stocks, the WISL behavioral apparatus and assay, courtship and phototaxis assays, antennal manipulations, electrophysiology, calcium response imaging and sample preparation, sound and wind stimuli and statistical methods are provided in the Supplementary Methods section.

METHODS

Fly stocks

Flies carrying *JO-ACE*, *JO-CE*, *and JO-AB* were described in Kamikouchi et al.7. *UAS-GCaMP*24, 25 and *UAS-mCD8-GFP* flies were obtained from Y. Wang and R. Axel, *UAS-FRT-STOP-FRT-Ricin* flies26 were obtained from D. Berdnik, JO-CE-GAL4; eyFLP flies were obtained from H. Inagaki, *Canton-S* flies from J. Dubnau, and *UAS-hid* flies from B. Hay. Flies were maintained on corn meal-molasses food at 25°C on a (12/12) light-dark cycle.

WISL behavioral apparatus

The WISL assay was performed in a 6 × 6 × 1.5 cm transparent acrylic plastic box (WISL chamber), which has airflow inputs and outputs (1 cm diameter) on two of the four vertical sides of the box. The input tubing carries airflow from a tank containing breathable air, connected to a flow regulator. The output tubing allows the airflow to escape from the box, and is connected to a flow meter that measures the speed of the airflow. The WISL chamber was mounted on a transparent plastic table and was trans-illuminated with a fluorescent light from underneath. A video camera (Sony, DCR-HC40 NTSC) was set up above the WISL chamber to record the flies' locomotor activity.

WISL assay protocol

20 flies per trial were sorted 36–48 hours prior to testing, using nitrogen gas or cold anesthesia. On the testing day, 20 flies were aspirated into the WISL chamber and allowed to acclimate for 7–8 min just before initiating the trial. A standard WISL trial lasts for 270 seconds. Flies are given a brief mechanical stimulation (5 manual strikes on the table that the WISL chamber was mounted on) at 55 seconds, and airflow exposure begins at 80 seconds and ends at 120 seconds. Locomotor activity was recorded at 10 frames/second and average velocity was computed using custom software written in a Matlab (MathWorks Inc.).

Courtship (female receptivity) assay

Naive *Canton-S* males and virgin females of the genotype of interest were collected immediately after eclosion, using nitrogen or CO_2 gas anesthesia. Naive males were individually housed while virgin females were group housed for 6 days until the test day. Single naive *Canton-S* male and a single virgin female of the genotype of interest were placed in a mating chamber (1 X 1 X 0.4cm square chamber), and the time at which a

successful copulation occurred was recorded for each mating pair. Successful copulation typically lasts 15–25 minutes.

Phototaxis assay

40 flies per trial were sorted 48 hours prior to testing, using nitrogen or CO_2 gas anesthesia. On the test day, 40 flies were tapped into the elevator of a T-maze and allowed to rest for one minute in a dark. Then, elevator was lowered to the choice point where flies were given one minute to make a choice between a dark tube, or a tube illuminated with a 40W fluorescent light, positioned approximately 20 cm away. The phototaxis response was analyzed by calculating the PI using the following formula: PI = [(2* COR)−1] *100. COR= (number of flies that chose the illuminated tube/total number of flies). PI = 0 indicates an equal distribution of flies between the dark and illuminated tubes. PI = 100% indicates that all flies chose the illuminated tube.

Antenna manipulations

In order to test the role of Johnston's organ in wind detection, a3 segments were surgically removed using a pair of forcepts, 48 hours prior to the WISL testing. For the antennal gluing experiment, a small drop of UV-activated glue was placed at the junction between the a2 and a3 segments bilaterally, and cured with a UV lamp for 3–5 seconds, 48 hours before the testing. For the mechanical probe antennal displacement experiment, a sharpened tungsten needle was used to move the aristae in different direction and patterns. The probe was mounted on a DC motor/controller (LTA-HS and SMC100CC, Newport), which was controlled by custom Matlab software (MathWorks Inc). To push the aristae backward, the probe was positioned anterior to the aristae; conversely, to push the aristae forward the probe was positioned posterior to the aristae. In the 'push back' (and 'push forward') conditions, the aristae were pushed backward (and forward) in a single increment of varying distances (either 0.01, 0.02, 0.025, 0.03, 0.04, 0.05, 0.07, 0.09, or 0.11mm), held for 8 seconds in the displaced position and then returned to the original position. In another experiment, the aristae was pushed backwards in three successive steps of 0.033mm (a total of 0.099mm), held in place for 2.9 seconds after each successive step, and then returned to the original position. In all conditions, the probe and aristae movements were verified using a video camera (GE680, Proscillica) that was set up underneath the fly preparation mounted on the microscope stage as describe above.

Electrophysiology

Extracellular recordings from Johnston's organ axons were recorded at the a1/a2 joint using a tungsten or glass electrode (0.5 MΩ) as described in Eberl et al.14 in a sound-proof chamber. Pulse song segments of recorded *D. melanogaster* courtship song (provided by J. Hall23 and D. Eberl) were used as the sound stimulus and an airflow rate between 0.3–0.9m/second was used as the wind stimulus.

Calcium response imaging and sample preparation

Flies were anesthetized in a plastic vial on ice for 15~20 sec, and were then gently inserted into a hole of a thin plastic rectangular plate. Small drops of wax (55°C) were applied to

prevent the fly from moving out from the hole. After the fly was stabilized in the plastic hole, the preparation was oriented in an up-side-down position (see Fig. 2b). The proboscis, ventral part of thorax and abdomen, and legs are protruding from the upper side of the horizontal plane of the plastic, while the rest of the fly head (including the antennae, but excluding the proboscis), thorax, and dorsal part of abdomen were protruding from the bottom side of the horizontal plane of the plastic. In a saline bath, the proboscis was cut off and the area surrounding the proboscis was surgically removed to expose the ventral side of the brain. Fat and air sacs were gently removed to have a clear view of the brain. For calcium response imaging, the water immersion objective lens (40X, N.A.=0.8, Olympus) was lowered near the exposed brain, while the underside of the plastic specimen mount, which contained the intact antennae, was kept dry and exposed to wind and sound stimuli.

Sound stimuli used in these experiments were recorded segments (provided by J. Hall23 and D. Eberl) of the pulse song portion of *D. melanogaster* courtship song, played at 75–100dB at the aristae using a loudspeaker (ProMonitor 800 loudspeaker, Definitive Technology) and amplifier (P.A. amplifier, Radioshack) and was measured using a digital sound meter (DSM-325, Mannix). We tested the frequency tuning of zones A and B using narrowband signals derived from the original pulse-song. The original pulse-song was filtered in order to set the center of the frequency spectrum at a desired frequency between 100 and 2000 ±200 Hz (using the Fourier transformation).

Wind stimuli used in imaging experiments were delivered at speeds between 0.005–15 m/sec. Wind speed was controlled by flow regulator (mass flow meters and controllers – Smart Trak series 100, Sierra Instrument Inc.) and was measured using an anenometer (Testo-435, Testo GmbH & Co.). VClamp software (Pairie Technology) was used to control all aspects of sound and wind stimuli used in the imaging experiments.

All imaging was performed on an Ultima two-photon laser scanning microscope (Prairie Technology). Live images were acquired at 6.1 frames per second using Olympus 40X (N.A.=0.8) water immersion objective at 128×128 resolution with an imaging wavelength at 925 nm. GCaMP responses were quantified using custom software written in MatLab. The relative change in fluorescence intensity (ΔF/F) was computed by first calculating the average pixel values in the region of interest (ROI) during the experimental period and applying a three frame moving average smoothing function. This average fluorescence value, F_{av}, was then converted to ΔF/F using the formula $\Delta F/F = (F_{av}-F_0)/F_0$, where F_0 is the baseline fluorescence value, measured as the average of frames 2–9. Average ΔF/F for specific stimulus period was compared between different JON zones to test for statistical significance by repeated measure ANOVA.

Supplementary Material

Refer to Web version on PubMed Central for supplementary material.

Acknowledgments

We thank Ulrike Heberlein and Fred Wolf (UCSF) for hosting a sabbatical that led to the discovery of WISL; J. S. Johnson for helpful discussions; Lihi Zelnik, Michael Reiser and Pietro Perona for creating locomotor tracking

software; Dan Eberl and Jeff Hall for *D. melanogaster* courtship song recordings; Gaby Maimon for making fly holders for imaging experiments; Mike Roy for building behavioral chambers for WISL and female receptivity assays; Hidehiko Inagaki for *JO-CE-GAL4;eyFLP* flies; Bruce Hay for *UAS-hid* flies, Daniela Berdnik for *UAS-FRT-STOP-FRT-Ricin* flies, Michael Dickinson for anemometers and helpful discussions; J.L. Anderson for advice on fluid mechanics; Martin Gopfert for providing a pressure gradient microphone; Mark Konishi for advice and use of lab facilities; and Gaby Mosconi for laboratory management. D.J.A. is an Investigator of the Howard Hughes Medical Institute. This work was supported in part by NSF grant EF-0623527.

References

1. Johnston, J.; Templeton, A. Dispersal and clines in Opuntia breeding Drosophila mercatorum and Drosophila hydei at Kamuela, Hawaii. In: Barker, JSF.; Starmer, WT., editors. Ecological Genetics and Evolution. Academic Press; Sydney: 1982. p. 241
2. Johnston J, Heed W. Dispersal of desert-adapted Drosophila: the saguaro-breeding D. Nigrospiracula. Am Nat. 1976; 110(974):629.
3. Budick SA, Reiser MB, Dickinson MH. The role of visual and mechanosensory cues in structuring forward flight in Drosophila melanogaster. J Exp Biol. 2007; 210(Pt 23):4092. [PubMed: 18025010]
4. Richardson R, Johnston J. Behavioral components of dispersal in Drosophila mimica. Oecologia. 1975; 20:287.
5. Caldwell JC, Eberl DF. Towards a molecular understanding of Drosophila hearing. J Neurobiol. 2002; 53(2):172. [PubMed: 12382274]
6. Kernan MJ. Mechanotransduction and auditory transduction in Drosophila. Pflugers Arch. 2007; 454(5):703. [PubMed: 17436012]
7. Kamikouchi A, Shimada T, Ito K. Comprehensive classification of the auditory sensory projections in the brain of the fruit fly Drosophila melanogaster. J Comp Neurol. 2006; 499(3):317. [PubMed: 16998934]
8. Nakai J, Ohkura M, Imoto K. A high signal-to-noise Ca(2+) probe composed of a single green fluorescent protein. Nature biotechnology. 2001; 19(2):137.
9. Gopfert MC, Robert D. The mechanical basis of Drosophila audition. J Exp Biol. 2002; 205(Pt 9): 1199. [PubMed: 11948197]
10. Mamiya A, Beshel J, Xu C, et al. Neural representations of airflow in Drosophila mushroom body. PLoS ONE. 2008; 3(12):e4063. [PubMed: 19115002]
11. Manning A. Antennae and sexual receptivity in Drosophila melanogaster females. Science. 1967; 158(797):136. [PubMed: 6054813]
12. Kim J, Chung YD, Park DY, et al. A TRPV family ion channel required for hearing in Drosophila. Nature. 2003; 424(6944):81. [PubMed: 12819662]
13. Wang SL, Hawkins CJ, Yoo SJ, et al. The Drosophila caspase inhibitor DIAP1 is essential for cell survival and is negatively regulated by HID. Cell. 1999; 98(4):453. [PubMed: 10481910]
14. Eberl DF, Hardy RW, Kernan MJ. Genetically similar transduction mechanisms for touch and hearing in Drosophila. J Neurosci. 2000; 20(16):5981. [PubMed: 10934246]
15. Tanouye MA, Wyman RJ. Motor outputs of giant nerve fiber in Drosophila. Journal of neurophysiology. 1980; 44(2):405. [PubMed: 6774064]
16. Bennet-Clark HC. Acoustics of insect song. Nature. 1971; 234:255.
17. Moffat KG, Gould JH, Smith HK, et al. Inducible cell ablation in Drosophila by cold-sensitive ricin A chain. Development (Cambridge, England). 1992; 114(3):681.
18. Wong AM, Wang JW, Axel R. Spatial representation of the glomerular map in the Drosophila protocerebrum. Cell. 2002; 109(2):229. [PubMed: 12007409]
19. Ewing AW. The antenna of *Drosophila* as a ‘love song’ receptor. Physiol Entomol. 1978; 3:33.
20. Ikeda I, Yamashita Y, Ono T, et al. Selective phototoxic destruction of rat Merkel cells abolishes responses of slowly adapting type I mechanoreceptor units. J Physiol (Lond). 1994; 479(Pt 2):247. [PubMed: 7799224]

21. Hoffmann JN, Montag AG, Dominy NJ. Meissner corpuscles and somatosensory acuity: the prehensile appendages of primates and elephants. The anatomical record Part A, Discoveries in molecular, cellular, and evolutionary biology. 2004; 281(1):1138.

22. Kamikouchi A, Inagaki HK, Effertz T, et al. The neural basis of *Drosophila* gravity sensing and hearing. Nature in press. 2008

23. Wheeler DA, Fields WL, Hall JC. Spectral analysis of Drosophila courtship songs: D. melanogaster, D. simulans, and their interspecific hybrid. Behavior genetics. 1988; 18:675–703. [PubMed: 3146969]

24. Wang JW, Wong AM, Flores J, Vosshall LB, Axel R. Two-photon calcium imaging reveals an odor-evoked map of activity in the fly brain. Cell. 2003; 112:271–282. [PubMed: 12553914]

25. Wang Y, Guo HF, Pologruto TA, Hannan F, Hakker I, Svoboda K, Zhong Y. Stereotyped odor-evoked activity in the mushroom body of Drosophila revealed by green fluorescent protein-based Ca2+ imaging. J Neurosci. 2004; 24:6507–6514. [PubMed: 15269261]

26. Berdnik D, Chihara T, Couto A, Luo L. Wiring stability of the adult Drosophila olfactory circuit after lesion. J Neurosci. 2006; 26:3367–3376. [PubMed: 16571743]

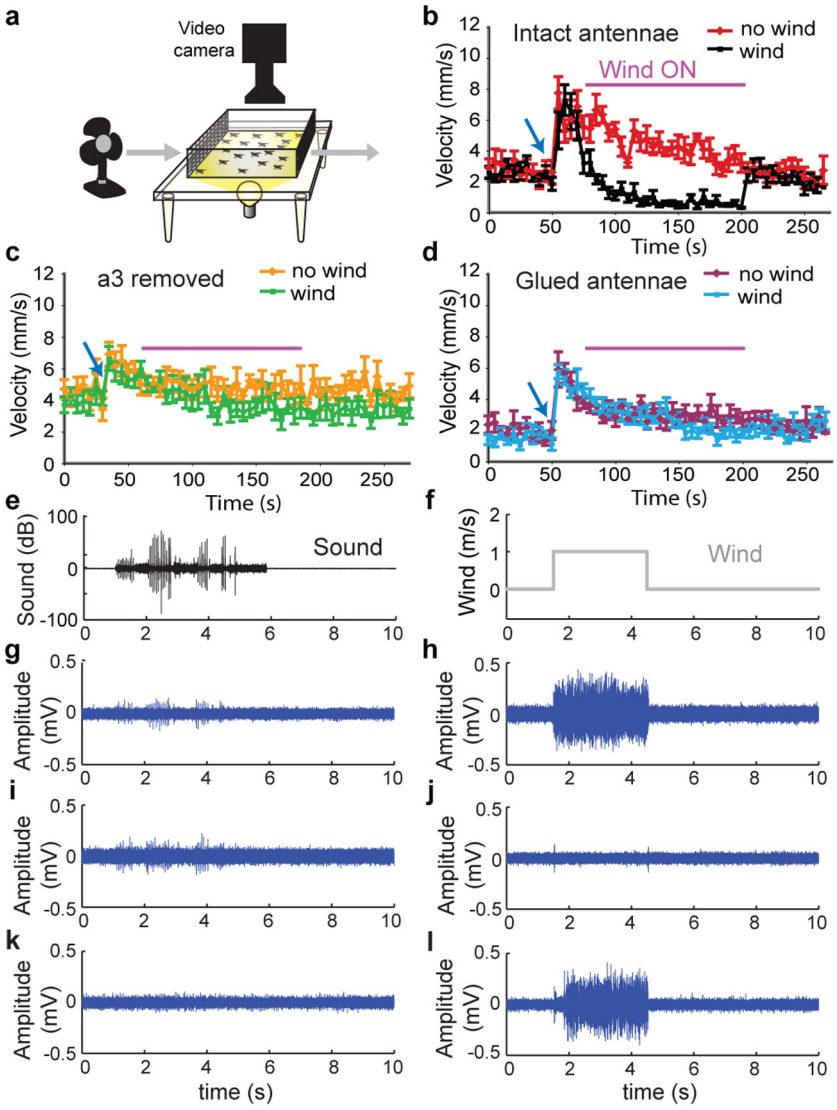

Figure 1. Behavioral and electrophysiological analyses of wind responses in *Drosophila*

(a) Schematic illustrating WISL assay (see Supplementary Methods). (b) WISL behavior in CS flies (Supplemental Movie 1). Data represent mean (±SEM) velocities (n=6). Blue arrow indicates brief mechanical startle. The “no wind” vs. “wind” curves are significantly different (p=.0001, Kruskal-Wallis ANOVA). (c, d) Elimination of WISL by removal of a3 (c) or gluing a3 to a2 (d). The “no wind” vs. “wind” curves are not significantly different (n=6). (e–l) Extracellular recordings of JO neuron responses (blue traces) to sound (e) or wind (f). (g, h) Response to both sound (g) and wind (h). (i, j) Response to sound (i) but not wind (j). (k, l) Response to wind (l) but not sound (k).

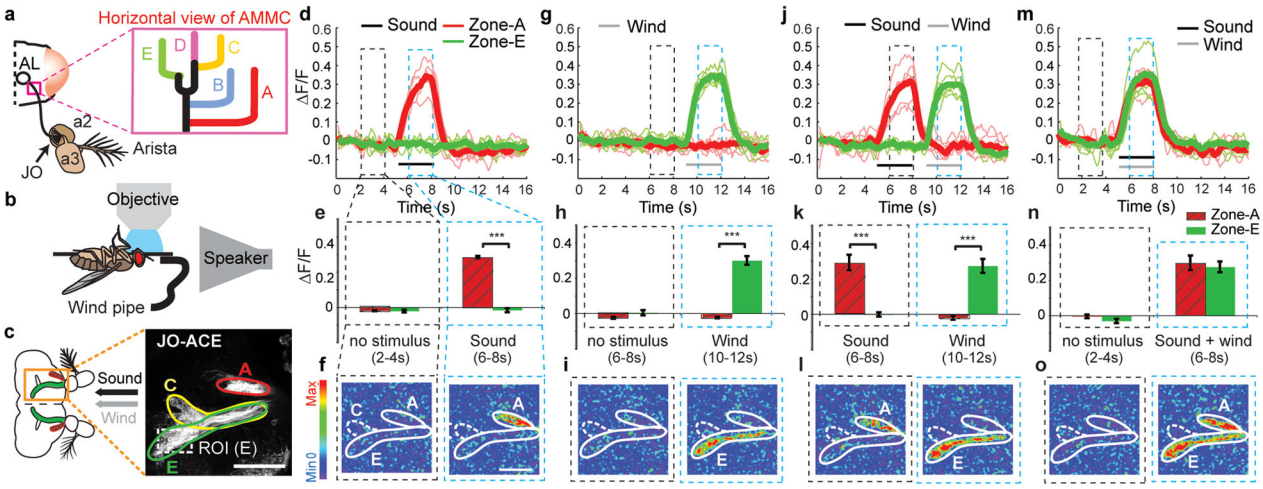

Figure 2. Calcium imaging reveals distinct populations of wind- and sound-responsive JO neurons

(a–c) Schematics illustrating (a) location of JO relative to a2 and a3, and five JO neuron axonal terminal zones7 in the AMMC; (b) imaging set-up. (c) Zones A, C, and E are visualized using a UAS-mCD8-GFP reporter. ROI, region of interest for ΔF/F measurements in zone E. (d–o) Zones A (red traces, hatched bars) and E (green traces, bars) are activated by sound and wind, respectively, whether presented singly (d–i), sequentially (j–l) or simultaneously (m–o) (see Supplemental movies 2a–e). Thick traces (d, g, j, m) represent average of the individual (thin) traces (n=6). (i–l) Bar graphs indicate the mean (±SEM) integrated ΔF/F in the time bins (dashed rectangles in d, g, j, m; see Methods). ***, $p<0.001$ (Repeated measure ANOVA and Bonferroni's planned comparisons). (f, i, l, o) ΔF images of GCaMP activation in zones A and E. Scale bars, 50μm.

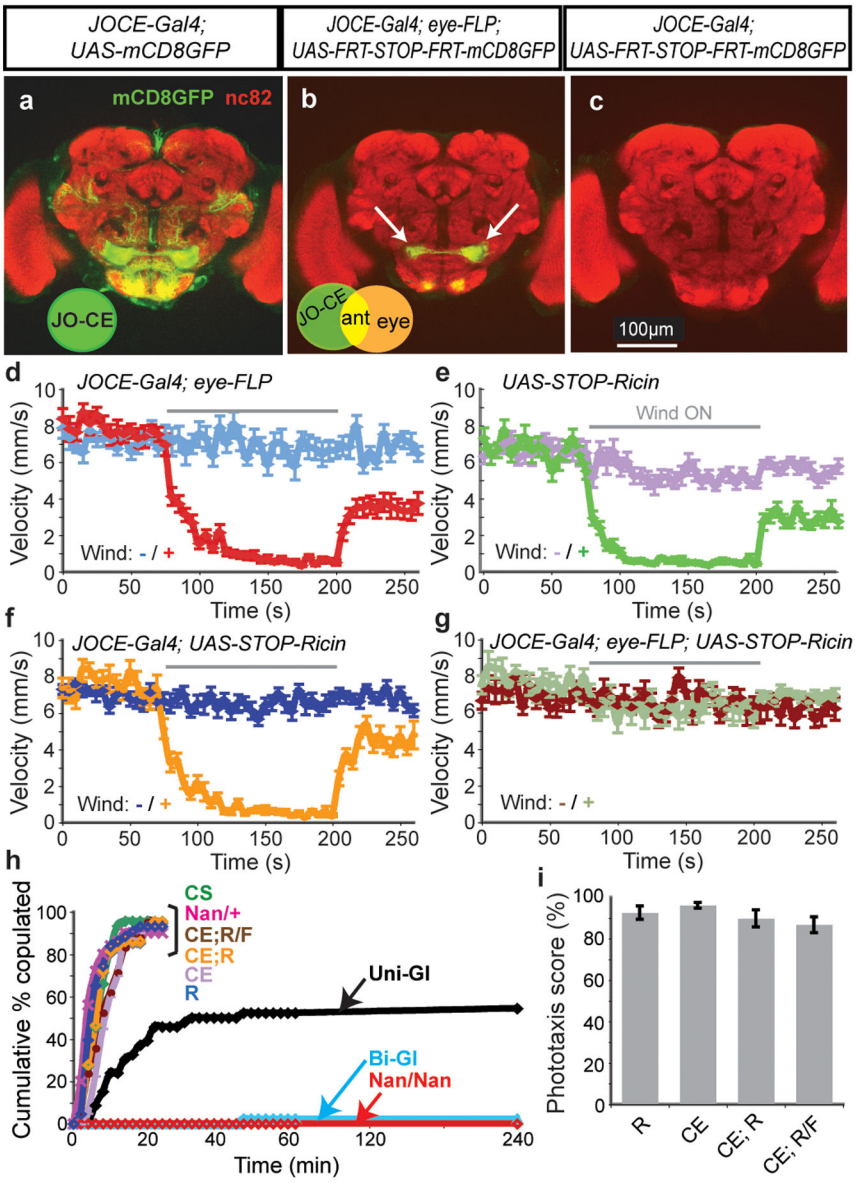

Figure 3. Ablation of wind-sensitive (C and E) neurons abolishes WISL behavior

(a–c) GFP expression patterns of the indicated genotypes, double-stained with antibodies to GFP (green) and nc82 (red). (a) Original JO-CE-Gal4 pattern. (b) Antennal-restricted JO-CE-Gal4 pattern using eye-FLP. Arrows indicate AMMC; underlying structures are gustatory neuron projections to the sub-oesophageal ganglia7. (c) Control for (b) lacking eye-FLP. (d–g) WISL analysis. Curves represent mean velocity±SEM (n=15). (d–f) Genetic controls show robust WISL. The “wind−” vs. “wind+” curves are significantly different ($p<0.0001$). (g) Ablation of C and E neurons abolishes WISL. (h) Cumulative percentage of manipulated females copulating with CS males. >90% of all pairs in bracketed conditions exhibited successful copulation within 20 min (n=40–50 pairs). Genotypes: CE; R/F = JO-CEGal4; UAS<STOP<Ricin/eye-FLP; CE; R = JO-CEGal4; UAS<STOP<Ricin; CE = JO-CEGal4; R = UAS<STOP<Ricin. Unilateral (“Uni-Gl”) or bilateral (“Bi-Gl”) gluing of the

aristae, or the *nanchung* mutation (*Nan/Nan*)12 impaired copulation ($p<0.0001$). Ablation of JO-CE neurons ("CE; R/F") did not impair either copulation (h), or phototaxis (i). Phototaxis scores represent mean±SEM (n= 7). P-values are shown by Kruskal-Wallis ANOVA.

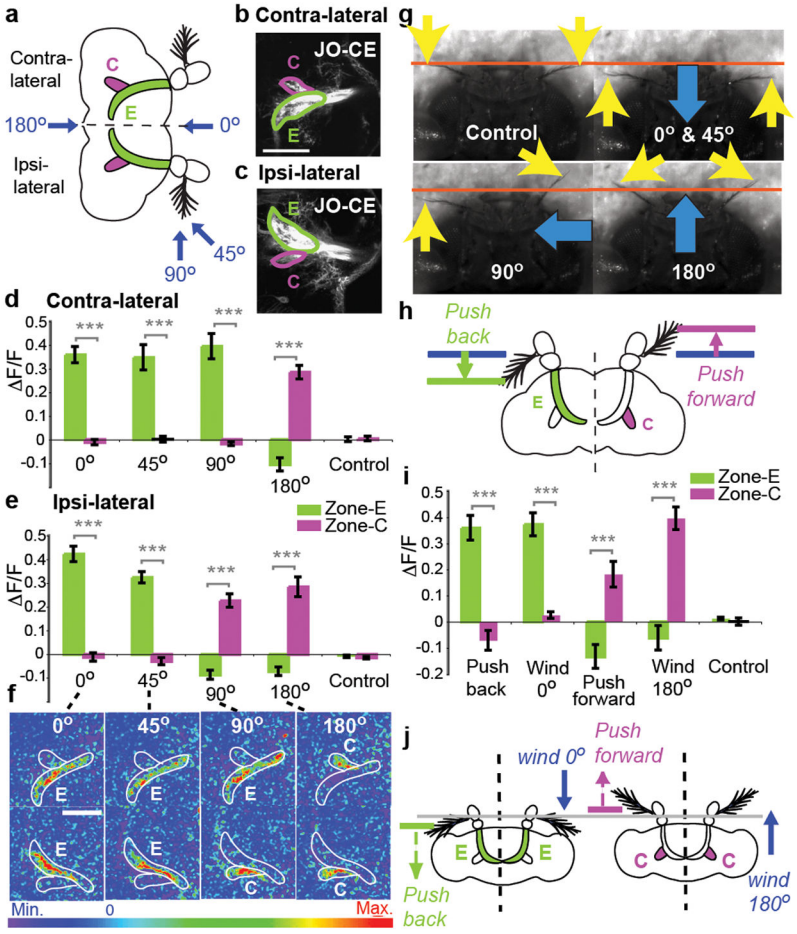

Figure 4. Wind direction-sensitivity of zones C vs. E

(a–c) Schematic (a) and mCD8-GFP expression (b, c) illustrating zones C and E in contra- and ipsi-lateral hemi-brains. Blue arrows indicate wind direction. (d–f) Average (±SEM) ΔF/F signals integrated over the stimulus period for zones C and E in the contra- (d) and ipsi- (e) lateral hemi-brains, and corresponding ΔF images (f; see Supplemental movies 3a–e). (g) Still frames from video recordings of aristae movements during wind stimulation (Supplemental movies 4a–e). Yellow arrows indicate aristae position, orange line denotes rest position (“Control”). Blue arrows indicate wind direction. (h) Schematic illustrating predicted responses of zones C and E to directional, probe-driven aristae displacements. (i) Responses of the C and E neurons to wind and directional arista displacements. (j) Summary illustrating differential sensitivity of zones C and E to direction of arista displacement. Scale bars, 50μm. ***, $p<0.0001$ (Repeated measures ANOVA and Bonferroni’s planned comparisons).

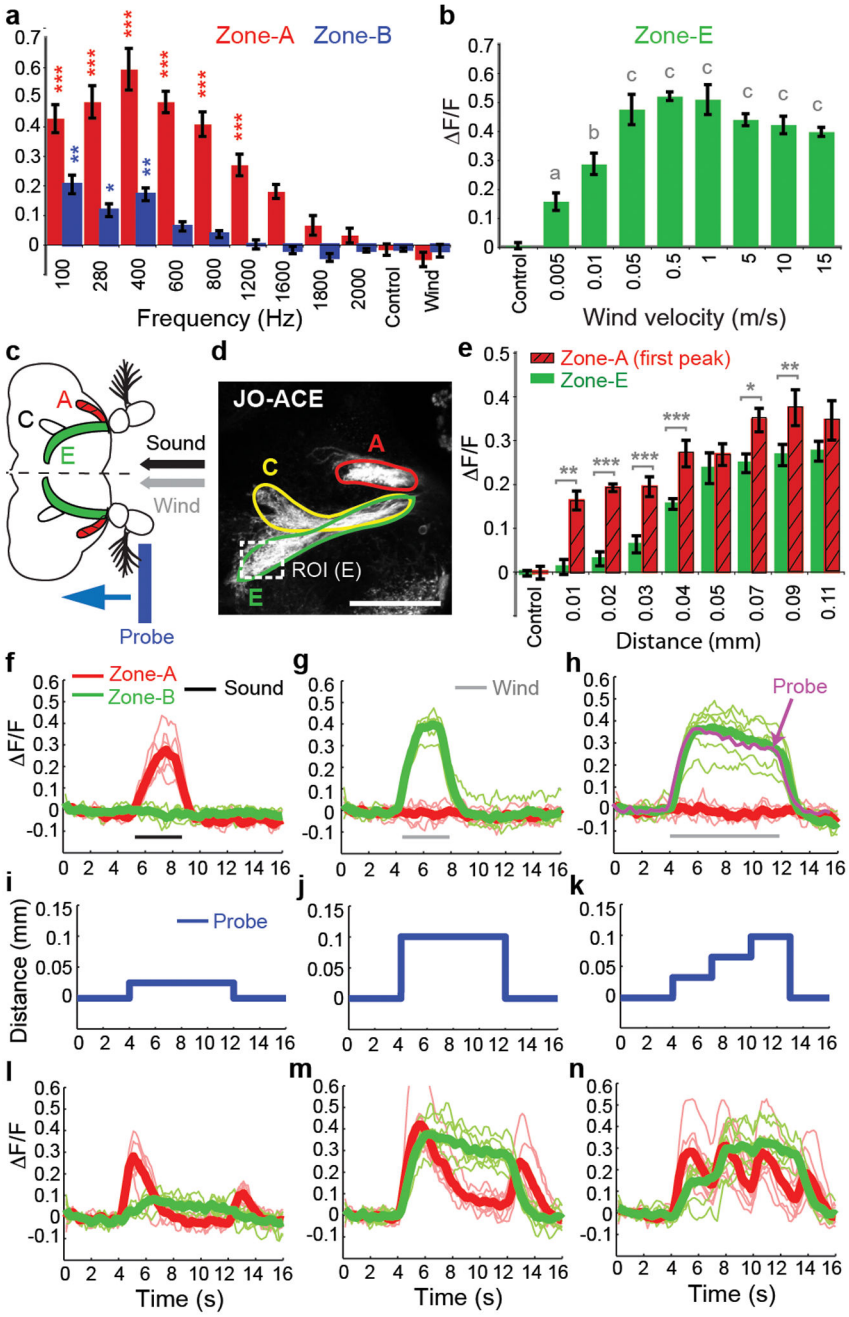

Figure 5. Wind- and sound-sensitive JO neurons have different intrinsic response properties

(a) Sensitivity of zones A and B to different sound frequencies (mean±SEM, n=6). *** (red), p<0.0001; * (blue), p<0.01; ** (Blue), p<0.001 relative to control. (b) Sensitivity of zone E to different wind speeds (n = 5). Letters indicate significant differences relative to control (all p<0.0001 except “a,” p<0.001). (c–n) Comparison of sound-, wind-, and probe-evoked responses in zones A and E. (c,d) Schematic (c) and mCD8-GFP expression (d) illustrating zones A, C and E. ROI, region of interest for ΔF/F measurements in zone E. Scale bar, 50μm. (e) Responses of zones A and E to different distances of probe-induced

arista displacement. *, p<0.01; **, p<0.001; ***, p<0.0001; all zone A responses (relative to control), p<0.0001 except 0.01 mm (p<0.001); all zone E responses ≥ 0.04 mm, p<0.0001; zone E responses < 0.04 mm not significant. (f–h) Sound and wind responses. Thick lines represent average of the individual (thin) traces (n=6). (h) Superposition of the average responses of zone E to 8 seconds of wind (green trace) and mechanical probe displacement (magenta trace; see m). (i–n) Responses (l–n) of zones A and E to different distances and patterns of probe-induced arista displacement (i–k) (n=6). All p-values are shown by Repeated measure ANOVA and Bonferroni multiple comparisons.